A strong seasonal dependence in the Martian hydrogen exosphere

Dolon Bhattacharyya, John T. Clarke, Jean-Loup Bertaux, Jean-Yves
Chaufray, Majd Mayyasi

HAL Id: insu-01218106

https://insu.hal.science/insu-01218106

Submitted on 7 Apr 2016

A strong seasonal dependence in the Martian hydrogen exosphere

Dolon Bhattacharyya[1], John T. Clarke[1], Jean-Loup Bertaux[2], Jean-Yves Chaufray[2], and Majd Mayyasi[1]

[1]Center for Space Physics, Boston University, Boston, Massachusetts, USA, [2]LATMOS/CNRS, Guyancourt, France

Abstract Hubble Space Telescope and Mars Express observed unexpected rapid changes in the Martian hydrogen exosphere involving a decrease in scattered Lyman α intensity in fall 2007 (solar longitude, $L_s = 331°–345°$). These changes detected were speculated to be a combination of seasonal variation and/or dust storms and lower atmospheric dynamics. Here we present Hubble Space Telescope observations of Mars in 2014 over a broad range of heliocentric distances and seasons ($L_s = 138°–232°$) which indicate a factor of ~3.5 change in Martian Lyman α brightness associated with a factor of ~5.4 variation of hydrogen escape flux in the absence of global dust storms and significant solar variability. We thus conclude that seasonal effects have a strong influence on the hydrogen exosphere, which in turn has major implications for the processes that control water supply to the Martian upper atmosphere and the history of water escape from Mars.

1. Introduction

Mars is believed to have been more Earth-like early in its history than it is today. There is considerable geological evidence that the planet's volatile inventory and climate have changed markedly throughout its evolutionary period [*Jakosky and Philips*, 2001; *Baker*, 2001]. Elevated ratios of atmospheric D/H at Mars arising from the difference in atomic mass between D and H provide evidence of escape of substantial amounts of hydrogen and thus water into space [*Owen*, 1992; *Bertaux and Montmessin*, 2001; *Villanueva et al.*, 2015]. However, the relative amounts of water that have escaped Mars or that remain frozen in its crust today are not well known. Early analysis of photochemistry of the planet suggested that most of the atmospheric water vapor is present below an altitude of 20 km, wherein it is photodissociated by solar ultraviolet (UV) radiation into its constituents, atomic hydrogen, and oxygen [*Hunten and McElroy*, 1970; *McElroy and Donahue*, 1972; *Parkinson and Hunten*, 1972]. The hydrogen thus created diffuses upward slowly in the form of H_2, a by-product of the recombination reaction producing a stable CO_2 atmosphere at Mars [*Hunten and McElroy*, 1970; *McElroy and Donahue*, 1972]. Once H_2 arrives in the ionosphere, it can be promptly dissociated by reactions with O_2^+ and CO_2^+ to form H, which then migrates upward forming the Martian exosphere [*Krasnopolsky*, 2002]. This exosphere was first detected by Mariner 6 and 7 through UV measurement of resonantly scattered solar Lyman α (121.57 nm) photons by hydrogen, at altitudes up to 30,000 km or ~8.8 R_{mars} [*Barth et al.*, 1969, 1971]. The high-energy tail of the thermal population of hydrogen atoms has enough energy to escape the gravitational pull of the planet, a phenomenon known as Jeans escape. This escape is substantial for H atoms compared with heavier atoms like oxygen, which mostly escape via nonthermal mechanisms like dissociative recombination [*McElroy*, 1972]. The slow diffusion of H_2 and its longer chemical lifetime would give rise to a stable escape flux over the course of the Martian year and seasons [*Hunten and McElroy*, 1970; *Hunten*, 1973].

The majority of H atoms in the Martian exosphere likely come from a population in thermal equilibrium with the collisionally dominated atmosphere (below 200 km) from which they originate. Therefore, an accurate determination of the mean temperature and exobase number density of the H population is essential for calculating its Jeans escape flux and is ascertained by modeling the resonantly scattered Lyman α emission from the exosphere of Mars. This Lyman α emission line is optically thick at the Martian line center (121.57 nm) leading to multiple scattering [*Anderson*, 1974]. Hence, analysis of the Mariner 6 and 7 Lyman α measurements was done using a radiative transfer model, coupled with a Chamberlain exosphere [*Anderson and Hord*, 1971]. The model results suggested an exobase density of $3 \pm 0.5 \times 10^4 \, cm^{-3}$ and a temperature of $350 \pm 100 \, K$ for median solar activity. The calculated temperature was higher than bulk atmospheric temperatures measured by other orbiting spacecraft and landers (temperature, $T = 145–220 \, K$) under different solar conditions [*Bougher et al.*, 2000; *LeBlanc et al.*, 2007], a disparity which could be explained by the presence of a two-component population of H in the Martian exosphere. The SPICAM and ASPERA instruments on MEX hinted at the presence of such a
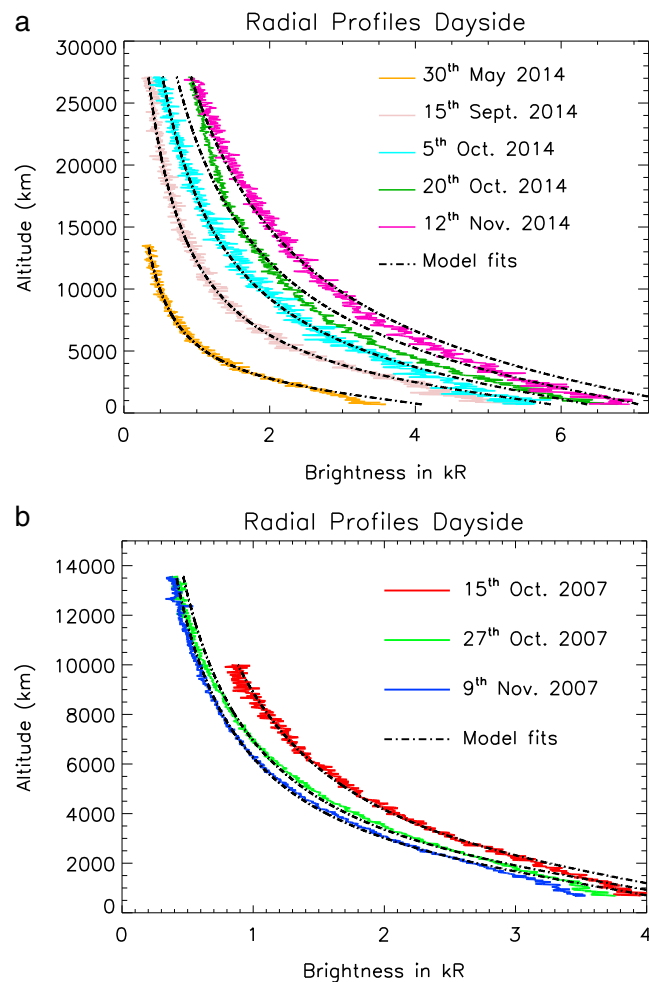
Figure 1. Radial brightness profiles in kilo Rayleighs with altitude for ± 45° from the subsolar point for the HST 2014 and 2007 observations along with their best two-component model fits. The level of Lyman α emission from exospheric hydrogen at Mars is observed to steadily increase with time in 2014 and decrease with time in 2007 at all altitudes.

population, with a thermal (cold) component at 200 K mixed with a superthermal (hot) component at $T > 500$ K formed by nonthermal processes like charge exchange with the solar wind, atmospheric sputtering, and molecular photodissociation among others, but had difficulties with absolute calibration [*Barabash and Lundin*, 2006; *Galli et al.*, 2006; *Chaufray et al.*, 2008]. However, recent observations of exospheric H made by the Rosetta spacecraft ($L_s = 189°$) have been analyzed using a modeled temperature of 260 K and no hot population [*Feldman et al.*, 2011]. This paper fit the optically thin Lyman β emission with a thermal component, supporting the presence of a "cold" component of H at the temperature of the neutral atmosphere. Their modeling of the Lyman α emission was uncertain since they did not take into account multiple scattering. Nevertheless, there still remains a poor understanding of the characteristics of the Martian exosphere and the actual escape flux of H from it.

In the course of constraining the H escape flux, observations of Mars by Hubble Space Telescope (HST) in October–November 2007 identified a 40% decrease in intensity of scattered solar Lyman α by Martian exospheric hydrogen in ~4 weeks [*Clarke et a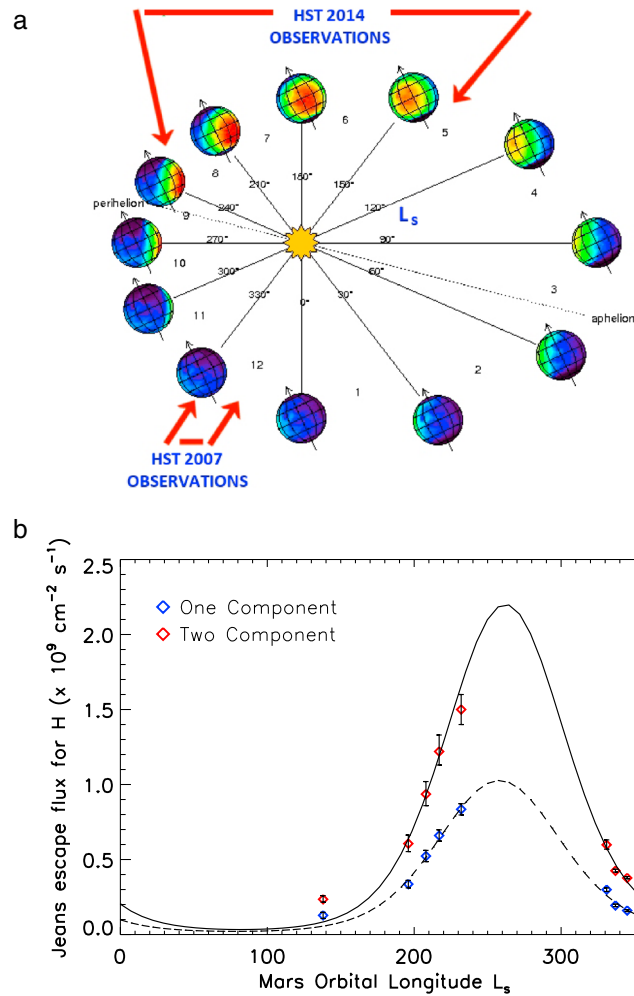l.*, 2014]. This trend, also observed by Mars Express over several months yielded up to an order-of-magnitude change in hydrogen escape flux [*Chaffin et al.*, 2014]. This variability was not accompanied by changes in solar flux or solar wind activity near solar minimum. It was concluded that the observed changes in H density and escape flux were brought about by intrinsic changes within the Martian atmosphere.

The process of resupplying hydrogen to the Martian exosphere through diffusion of molecular H_2 from below is slow (~10 to 500 days between altitudes of 10 and 100 km) and is not likely to produce the short-term changes observed during October–November 2007 [*Clarke et al.*, 2014]. Atmospheric models indicate that the increase in solar EUV flux in the upper atmosphere near perihelion could also lead to changes in the H escape flux [*Chaufray et al.*, 2015]. However, during the HST 2007 observations, Mars was moving away from the Sun ($L_s = 331°–345°$) coming out of southern summer, and the solar incident flux at Mars varied by ~5%, not enough to cause the observed decrease in ~4 weeks.

The presence of unexpectedly elevated levels of water vapor at high altitudes, higher than those predicted by Martian climate models, was found in the MEX data [*Maltagliati et al.*, 2011, 2013; *Fedorova et al.*, 2006, 2009]. Water vapor at high altitudes will undergo direct photodissociation by solar UV and bypass the slow diffusion process, which could lead to rapid changes in the hydrogen population in the Martian exosphere. SPICAM water vapor profiles obtained during the southern summer of Mars in year 29 (December 2007 to May 2009) showed densities of 50–100 ppm at altitudes of 60–80 km in both hemispheres, more than 10 times

Figure 2. (a) This figure shows the position of Mars at different solar longitudes (L_s) as well as the position of Mars around the Sun when the HST images were obtained (original image: http://www-mars.lmd.jussieu.fr/mars/time/solar_longitude.html). (b) This figure shows variation of hydrogen escape flux from Mars at various solar longitude positions. The single-component and the two-component escape fluxes have been fitted with a first-order relation to provide an approximation of the seasonal variation of hydrogen escape flux from Mars.

higher than predicted by models [*Maltagliati et al.*, 2011, 2013; *Fedorova et al.*, 2006, 2009]. Changes in water vapor quantities at high altitudes could be brought about by seasonal effects or Martian dust storm activity, which is season dependent [*Fedorova*, 2009; *Maltagliati*, 2013]. A major global dust storm occurred in June 2007 at Mars, with the dust opacity decreasing from ~0.8 to 0.2 through the following months overlapping with the HST and MEX observations [*Montabone et al.*, 2012]. The 2007 observing campaign followed this storm and showed a decrease in H density that could have been caused by either seasonal changes or the dust storm or a combination of both.

2. Observations

To resolve the effect of seasons and/or dust storms, a series of HST observations were undertaken in 2014 over a broad range of L_s values and heliocentric distances (Figure 1). These images were obtained in the far ultraviolet with the ACS-SBC instrument on board HST in five separate visits. The first observation was taken on 30 May 2014 ($L_s = 138°$) when Mars was coming out of northern summer solstice ($L_s = 90°$). The next set of observations were conducted during September–November 2014 ($L_s = 197°$–232°) with Mars close to perihelion ($L_s = 251°$) and approaching southern summer solstice ($L_s = 271°$) (Figure 2a). Dedicated HST observations of Lyman α emission from

the geocorona and interplanetary hydrogen were used to obtain an accurate background subtraction and zero level. The reduction pipeline is detailed in *Clarke et al.* [2009], and the adaptation to Mars is elaborated in *Clarke et al.* [2014]. The incident solar flux at Mars increased by 31.5% from 30 May to 12 November due to Mars' position in its orbit (Table 1).

Radial profiles of brightness (in kilo Rayleighs) versus altitude (670–35,000 km) were constructed for each of the HST observations over ±45° from the subsolar point. The calibration factor used for the HST data is specific for Lyman α (0.002633 counts/pixel s kR), an update from the band-pass-averaged value (0.002103 counts/pixel s kR) used in *Clarke et al.* [2014]. This value was determined by modeling the sensitivity of ACS with wavelengths within the band pass [*Avila et al.*, 2015; *Gustin et al.*, 2012] (supporting information). The intensity of Lyman α emission increased steadily with decreasing heliocentric distance, the same trend with distance observed in October–November 2007 (Figure 1) when Mars was receding from the Sun. The optically thick Lyman α emission has been modeled using a radiative transfer code to include multiple scattering effects.

Table 1. Observations and Modeled H Escape Flux Values[a]

Observation Date (Day of Year)	L_s	$F_0 \times 10^{11}$ (photons/cm^2/s/Å)	Distance to Sun (AU)	Single-Component ϕ_{jeans} ($\times 10^8$ cm^{-2} s^{-1})	Two-Component ϕ_{jeans} ($\times 10^8$ cm^{-2} s^{-1})
10/15/2007 288	331°	1.325	1.49	2.99 ± 0.12	5.98 ± 0.3
10/27/2007 300	337°	1.293	1.50	1.94 ± 0.08	4.25 ± 0.1
11/09/2007 313	345°	1.255	1.52	1.6 ± 0.06	3.77 ± 0.07
05/30/2014 150	138°	1.398	1.57	1.28 ± 0.2	2.35 ± 0.22
09/15/2014 258	197°	1.707	1.43	3.36 ± 0.25	6.06 ± 0.55
10/05/2014 278	208°	1.709	1.41	5.23 ± 0.37	9.36 ± 0.84
10/20/2014 293	217°	1.752	1.40	6.6 ± 0.37	12.2 ± 1.0
11/12/2014 316	232°	1.838	1.39	8.35 ± 0.37	15.0 ± 1.0

[a]Line-integrated flux obtained from the SORCE database [*Rottman et al.*, 2006] have been corrected for solar rotation and converted to line center flux [*Emerich et al.*, 2005].

3. Modeling and Analysis

The radiative transfer model used in this analysis is coupled with a Chamberlain exosphere [*Chamberlain*, 1963] and is based on *Chaufray et al.* [2008]. It utilizes the assumptions of *Thomas* [1963] and has two free parameters, exospheric density, and temperature. The model simulates the effect of multiple scattering in an optically thick atmosphere of $\tau < 200$ at line center. The modeled intensities are convolved with the instrument Point Spread Function for comparison with the HST data (supporting information).
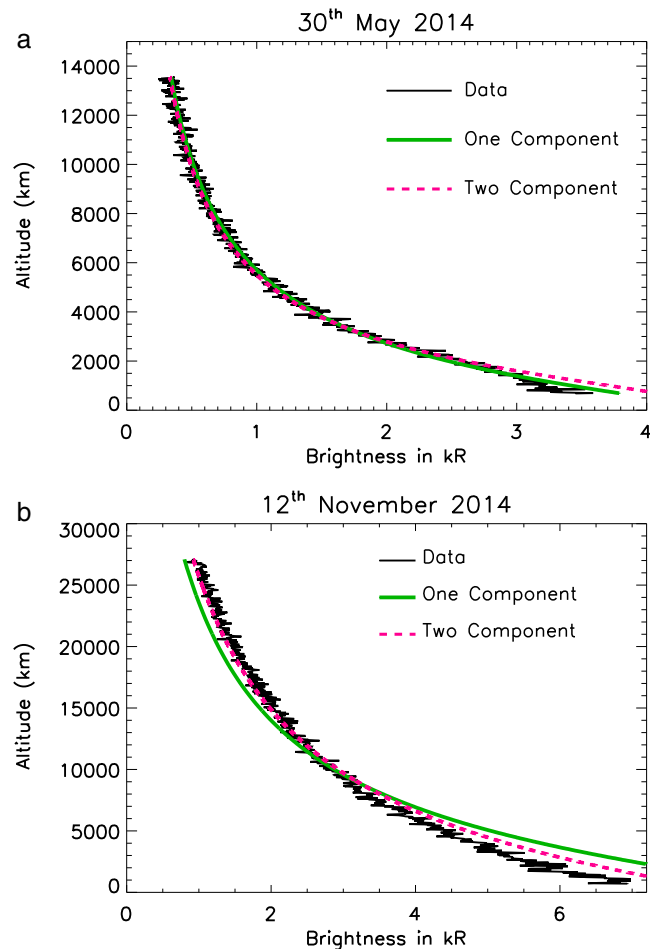
3.1. Single-Component Model

The altitude profiles were first modeled assuming a single thermal hydrogen population in the Martian exosphere. Simulations were done using various combinations of temperatures ranging from 170 to 440 K and exobase number densities from 10^4 to 5×10^5 cm^{-3}, the two free parameters of the model. The best fit to all the HST observations was obtained by minimizing χ^2 deviations between data and model. It is difficult to ascertain the modeling uncertainties due to various undetermined inherent assumptions about the characteristics of the Martian exosphere, like spherical symmetry of the density profile, a single Maxwellian distribution, and isothermal conditions in the day and night sector. Ignoring modeling uncertainties while calculating χ^2 values increases it beyond 1 (supporting information). For example, a modeling uncertainty 10 times larger than the observed uncertainty allows $\chi^2 < 100$ to be acceptable.

The best fit modeled temperatures for the 2007 observations at low solar activity ($F_{10.7} \sim 70$ at 1 AU) and the 2014 observations at high solar activity ($F_{10.7} \sim 144$) ranged from 360 to 440 K (Table 2), close to the values obtained by

Table 2. Model Fits to the Data

	Single-Component Model			Two-Component Model[a]			
Date of Observation	T_{exo} (K)	n_{exo} (cm^{-3})	χ^2_{red}	T_{cold} (K)	n_{cold} (cm^{-3})	n_{hot} (cm^{-3})	χ^2_{red}
10/15/2007	440	24,000 ± 1,000	5.69	170	105,000 ± 3,000	12,300 ± 600	7.6
10/27/2007	380	25,000 ± 1,000	6.73	170	96,000 ± 2,000	8,700 ± 200	17
11/09/2007	360	25,000 ± 1,000	5.65	170	91,000 ± 1,000	7,700 ± 200	16
05/30/2014	365	19,000 ± 3,000	2.23	200	47,000 ± 1,000	4,600 ± 400	4.1
09/15/2014	440	27,000 ± 2,000	3.48	200	71,000 ± 4,000	12,200 ± 1,100	2.3
10/05/2014	440	42,000 ± 3,000	7.10	230	66,000 ± 5,000	18,500 ± 1,500	2.6
10/20/2014	440	53,000 ± 3,000	20.36	240	85,000 ± 5,000	23,800 ± 2,000	7.8
11/12/2014	440	67,000 ± 3,000	20.71	240	97,000 ± 7,000	29,400 ± 2,000	5.1

[a]Temperature of the hot component is taken to be a constant, $T_{hot} = 800$ K.

Figure 3. The plot above show the comparison between best fit model runs to the HST data with a single population of H atoms and a hot + cold population of H atoms (two components).

Anderson and Hord [1971], *Dostovalov and Chuvakhin* [1973] for high solar activity ($F_{10.7} \sim 180$), and *Babichenko et al.* [1977] for low solar activity ($F_{10.7} \sim 60$). These temperatures are much higher than the bulk atmospheric temperatures estimated from UV CO_2^+, Cameron bands, N_2 Vegard-Kaplan bands and aerobraking measurements at low solar activity [*LeBlanc et al.*, 2006, 2007; *Bougher et al.*, 2000]. Such high temperatures obtained for the hydrogen population do not agree with Lyman β measurements (260 K) by *Feldman et al.* [2011] around solar minimum. They also do not agree with spacecraft drag measurements [*Forbes et al.*, 2008], which, however, have their own challenges [*Krasnopolsky*, 2010]. Martian global circulation models (MGCM) cannot explain temperatures greater than 440 K in the exosphere as this is not supported by the energy balance of the upper atmosphere [*Chaufray et al.*, 2015; *Bougher et al.*, 1999, 2009, 2015]. Therefore, a two-component population of H, with a small percentage at a higher temperature, was deemed to be the more likely scenario. Such a population detected at Venus has a similar effect of broadening the Martian Lyman α line like a single component at a high temperature [*Anderson*, 1976; *Bertaux et al.*, 1977; *Hodges*, 1999; *Chaufray et al.*, 2012].

3.2. Two-Component Model

The two-component model is a combination of a cold component at thermal equilibrium with the lower atmosphere (below 200 km) and a "hot" superthermal component created by nonthermal processes which dominate at higher altitudes. The superthermal component is taken to exist only beyond the exobase and approximated by a Maxwellian. For each observation the mean temperature of the thermal component is determined based on the conditions of the lower atmosphere simulated by an MGCM [*Forget et al.*, 1999; *Gonzalez-Galindo et al.*, 2009]. Different exobase number density combinations (1×10^4 to 5×10^5 cm^{-3})

within ranges predicted by photochemical models [*Krasnopolsky*, 2002; *Fox*, 2003] for H at Mars have been used to find the best fit modeled density by minimizing the χ^2 deviations to simulate the data for the predetermined thermal temperature. The temperature of the hot component was derived by assuming an optically thin atmosphere above 10,000 km dominated by superthermal atoms. Different combinations of exobase density (1×10^2 to $5 \times 10^4\,cm^{-3}$) and temperature (500–1000 K) within ranges predicted from MEX data [*Chaufray et al.*, 2008] were used to generate radial intensities, which were then fit to the data beyond 10,000 km. A series of best fit temperatures were obtained for all the HST observations through χ^2 minimization, and the temperature of the hot component was fixed to be the lowest temperature (800 K), common to all observations. Then the exobase number density for the superthermal component at 800 K was derived by minimizing χ^2 values for the model fits to the data (Table 2). The total number density profile (hot + cold), generated from the exobase temperature and density values for both the components, was then run through the RT model at the temperature of the cold component, deemed to be the majority, to obtain the final fit to the data (Figure 1). The discrepancies between data and model are smaller than the increasing trend in H brightness and are likely due to inherent model assumptions about the exosphere of Mars. Other combinations of hot and cold temperatures may provide good fits to the data, but given the lack of knowledge on the actual velocity distribution of hydrogen, arbitrary combinations of temperature and density were not modeled.

Figure 3 provides a comparison between a single-component and a two-component fit to the data for 30 May and 12 November 2014. Both models give a good fit to the data on 30 May 2014, when Mars was far from the Sun, while the two-component fit is better on 12 November 2014, when Mars was closer to the Sun and the emission was brighter. The reduced χ^2 values for the fits in Table 2 also indicate that the two-component model is better when Mars is closer to the Sun, thereby suggesting that the hot component may be related to the solar EUV flux or solar wind.

4. Discussion

The presence or absence of a superthermal component can significantly alter the Jeans escape flux of hydrogen from the exosphere of Mars as illustrated in Figure 2b. For example, the Jeans escape flux in the presence of a superthermal component is ~84% higher than a single-component scenario for 30 May 2014 and ~80% higher for 12 November 2014. Considering the presence of a thermal and a superthermal component of H in the Martian exosphere to be more likely, the Jeans escape flux calculated from the best fit exobase temperature and number density increased by a factor of ~5.4 between 30 May and 12 November 2014 (Table 1). No major changes in solar activity were recorded during the 2014 observations even though the solar cycle was close to solar maximum except for a medium solar flare (M7 class) during the passage of comet Siding Spring over 19/20 October 2014. The HST data taken during the comet encounter indicate a negligible change in Martian exospheric Lyman α intensity (<5%), and most observed changes are consistent with variations in the solar Lyman α flux. In 2007, the escape flux decreased by 37% within 4 weeks as Mars was moving away from the Sun with no significant changes in solar activity with the solar cycle near its minimum. Even though a global dust storm was recorded in June 2007 and only regional dust storm activity observed in 2014 (http://themis.mars.asu.edu/dust_maps), a significant increase in Martian exospheric Lyman α intensity was observed in 2014 indicating seasonal effects. Seasonal changes have also been observed in pickup ions of exospheric origin at Mars, as well as reflected solar wind ions at the bow shock [*Yamauchi et al.*, 2015]. Simulations using an MGCM for nonuniform exobase conditions found that the H escape flux was not diffusion limited but was directly dependent on the seasonal increase in incident solar EUV flux at the Martian upper atmosphere [*Chaufray et al.*, 2015]. However, the H escape flux at solar maximum between $L_s \sim 140°$–230° derived from the MGCM showed an increase of a factor of ~2.1 ($F_{10.7} \sim 220$), which is less than the factor of ~5.4 ($F_{10.7} \sim 144$) obtained with the HST 2014 data for the same L_s range (Table 1).

To estimate the functional form of these seasonal changes, the variation of H escape flux with L_s determined from the HST data can be represented by a simple sinusoid;

$$\phi_{Jeans}(L_S) = 10^{A Sin\left(\frac{2\pi L_S}{360°} + \varphi\right) + B} \tag{1}$$

Here $A = 0.84$, $B = 8.16$, and $\varphi = 3.35$ radians from the best fit to the single-component escape flux and $A = 0.91$, $B = 8.43$, and $\varphi = 3.28$ radians (Figure 3b) for the best fit to the two-component escape flux. While the existence of a strong seasonal variation is well established, the shape of the curve is only partially

constrained due to the thinly sampled data set and includes both solar minimum and maximum conditions. The observed seasonal variation of a factor of ~5.4 in ~6 months greatly exceeds the steady diffusion limited process previously assumed [*Hunten*, 1973]. The new observations suggest that seasons are important drivers of H escape, although the relative contribution of dust storms has yet to be determined. The relative importance of (a) water in the lower atmosphere and (b) solar EUV flux/dynamics can be found by further observations of H escape over the northern summer, when Mars moves farther from the Sun, but the surface atmospheric density shows a second maximum. Finding a second increase in the hydrogen brightness over $L_s = 0°–90°$ would implicate surface conditions as the primary driver of the changes in H escape flux, as opposed to control by the solar EUV flux which would decrease with increasing heliocentric distance.

Geological evidence has indicated that today's dry and cold Mars was warm and wet when Mars was young [*Jakosky and Philips*, 2001; *Baker*, 2001]. The water lost into space after the loss of its magnetic field [*Jakosky and Philips*, 2001] has been estimated from the present hydrogen escape flux for the Martian atmosphere. Earlier work assumed that this escape flux was diffusion limited and changed slowly over a Martian year [*Hunten*, 1973]. Here we present strong observational evidence for a large and persistent seasonal variation in H escape flux from Mars. Existing estimates of the Martian water reserves will have to be updated to reflect this, and a simple extrapolation of the present-day escape flux would not suffice to trace the historic escape of water from Mars and the depth of its primordial ocean.

References

Anderson, D. E. (1974), Mariner 6, 7 and 9 ultraviolet spectrometer experiment: Analysis of hydrogen Lyman alpha data, *J. Geophys. Res.*, *79*, 1513–1518, doi:10.1029/JA079i010p01513.

Anderson, D. E. (1976), The Mariner 5 ultraviolet photometer experiment—Analysis of hydrogen Lyman alpha data, *J. Geophys. Res.*, *81*, 1213–1216, doi:10.1029/JA081i007p01213.

Anderson, D. E., and C. W. Hord (1971), Mariner 6 and 7 ultraviolet spectrometer experiment: Analysis of hydrogen Lyman-alpha data, *J. Geophys. Res.*, *76*, 6666–6673, doi:10.1029/JA076i028p06666.

Avila, R., et al. (2015), ACS instrument handbook Version 4.0 (Baltimore: STScI).

Babichenko, S. I., E. V. Deregusov, V. G. Kurt, N. N. Romanova, V. A. Skliankin, A. S. Smirnov, J. J. Bertaux, and J. Blamont (1977), Measurements in interplanetary space and in the Martian upper atmosphere with a hydrogen absorption-cell spectrophotometer for L-alpha radiation on-board Mars 4-7 space probes, *Space Sci. Instrum.*, *3*, 271–286.

Baker, V. R. (2001), Water and the Martian landscape, *Nature*, *412*, 228–236.

Barabash, S., and R. Lundin (2006), ASPERA-3 on Mars Express, *Icarus*, *182*, 301–307.

Barth, C. A., W. G. Fastie, C. W. Hord, J. B. Pearce, K. K. Kelly, A. I. Stewart, G. E. Thomas, G. P. Anderson, and O. F. Rape (1969), Mariner 6 ultraviolet spectrum of Mars upper atmosphere, *Science*, *165*, 1004–1005.

Barth, C. A., J. B. Pearce, K. K. Kelly, G. P. Anderson, and I. A. Stewart (1971), Mariner 6 and 7 ultraviolet spectrometer experiment: Upper atmosphere data, *J. Geophys. Res.*, *76*, 2213–2227, doi:10.1029/JA076i010p02213.

Bertaux, J. L., and F. Montmessin (2001), Isotropic fractionation through water vapor condensation: The deuteropause, a cold trap for deuterium in the atmosphere of Mars, *J. Geophys. Res.*, *106*, 32,879–32,884, doi:10.1029/2000JE001358.

Bertaux, J. L., J. E. Blamont, A. I. Dziubenko, V. G. Kurt, T. A. Miziakina, E. N. Mironova, N. N. Romanova, and A. S. Smirnov (1977), Investigation of scattered Lyman alpha radiation in the vicinity of Venus, *CosRe*, *14*, 799–816.

Bougher, S. W., S. Engel, R. G. Roble, and B. Foster (1999), Comparative terrestrial planet: 2. Solar cycle variation of global structure and winds at equinox, *J. Geophys. Res.*, *104*, 16,591–16,611, doi:10.1029/1998JE001019.

Bougher, S. W., S. Engel, R. G. Robie, and B. Foster (2000), Comparative terrestrial planet thermospheres: 3. Solar cycle variation of global structure and winds at solstices, *J. Geophys. Res.*, *105*, 17,669–17,692, doi:10.1029/1999JE001232.

Bougher, S. W., T. M. McDunn, K. A. Zoldak, and J. M. Forbes (2009), Solar cycle variability of Mars dayside exospheric temperatures: Model evaluation of underlying thermal balances, *Geophys. Res. Lett.*, *36*, L05201, doi:10.1029/2008GL036376.

Bougher, S. W., D. J. Pawlowski, J. M. Bell, S. Nelli, T. Mcdunn, J. R. Murphy, M. Chizek, and A. J. Ridley (2015), Mars global ionosphere-thermosphere model: Solar cycle, seasonal, and diurnal variations of the Mars upper atmosphere, *J. Geophys. Res. Planets*, *120*, 311–342, doi:10.1002/2014JE004715.

Chaffin, M. S., J.-Y. Chaufray, I. Stewart, F. Montmessin, N. M. Schneider, and J.-L. Bertaux (2014), Unexpected variability of Martian hydrogen escape, *Geophys. Res. Lett.*, *41*, 314–320, doi:10.1002/2013GL058578.

Chamberlain, J. W. (1963), Planetary coronae and atmospheric evaporation, *Planet. Space Sci.*, *11*, 901–960.

Chaufray, J. Y., J. L. Bertaux, E. Quemerais, E. Villard, and F. LeBlanc (2012), Hydrogen density in the dayside Venusian exosphere derived from Lyman-α observations by SPICAV on Venus Express, *Icarus*, *217*, 767–778.

Chaufray, J.-Y., J.-L. Bertaux, F. LeBlanc, and E. Quemérais (2008), Observation of the hydrogen corona with SPICAM on Mars Express, *Icarus*, *195*, 598–613.

Chaufray, J.-Y., F. Gonzalez-Galindo, F. Forget, M. A. Lopez-Valverde, F. Leblanc, R. Modolo, and S. Hess (2015), Variability of the hydrogen in the Martian upper atmosphere as simulated by a 3D atmosphere-exosphere coupling, *Icarus*, *245*, 282–294.

Clarke, J. T., et al. (2009), Response of Jupiter's and Saturn's auroral activity to the solar wind, *J. Geophys. Res.*, *114*, A05210, doi:10.1029/2008JA013694.

Clarke, J. T., J.-L. Bertaux, J.-Y. Chaufray, G. R. Gladstone, E. Quemerais, J. K. Wilson, and D. Bhattacharyya (2014), A rapid decrease of the hydrogen corona of Mars, *Geophys. Res. Lett.*, *41*, 8013–8020, doi:10.1002/2014GL061803.

Dostovalov, S. B., and S. D. Chuvakhin (1973), On the distribution of neutral hydrogen in the upper atmosphere of Mars, *Cosmic Res.*, *11*, 767–773.

Emerich, C., P. Lemaire, J.-C. Vial, W. Curdt, U. Schühle, and K. Wilhelm (2005), A new relation between the central spectral solar H I Lyman α irradiance and the line irradiance measured by SUMER/SOHO during the cycle 23, *Icarus*, *178*, 429–433.

Fedorova, A., O. Korablev, J.-L. Bertaux, A. Rodin, A. Kiselev, and S. Perrier (2006), Mars water vapor abundance from SPICAM IR spectrometer: Seasonal and geographic distributions, *J. Geophys. Res.*, *111*, E09S08, doi:10.1029/2006JE002695.

Fedorova, A., O. I. Korablev, J.-L. Bertaux, A. V. Rodin, F. Montmessin, D. A. Belyaev, and A. Reberac (2009), Solar infrared occultation observations by SPICAM experiment on Mars-Express: Simultaneous measurements of the vertical distributions of H_2O, CO_2 and aerosol, *Icarus*, *200*, 96–117.

Feldman, P. D., et al. (2011), Rosetta-Alice observations of exospheric hydrogen and oxygen on Mars, *Icarus*, *214*, 394–399.

Forbes, J., F. G. Lemoine, S. L. Bruinsma, M. D. Smith, and X. Zhang (2008), Solar flux variability of Mars' exosphere densities and temperatures, *Geophys. Res. Lett.*, *35*, L01201, doi:10.1029/2007GL031904.

Forget, F., F. Hourdin, R. Fournier, C. Hourdin, O. Talagrand, M. Collins, S. R. Lewis, P. L. Read, and J.-P. Huot (1999), Improved general circulation models of the Martian atmosphere from the surface to above 80 km, *J. Geophys. Res.*, *104*(E10), 24,155–24,176, doi:10.1029/1999JE001025.

Fox, J. L. (2003), The effect of H_2 on the Martian ionosphere: Implications for atmospheric exolution, *J. Geophys. Res.*, *108*(A6), 1223, doi:10.1029/2001JA000203.

Galli, A., P. Wurz, H. Lammer, H. I. M. Lichtenegger, R. Lundin, S. Barabash, A. Grigoriev, M. Holmström, and H. Gunell (2006), The hydrogen exospheric density profiles measured with ASPERA-3/NPD, *Space Sci. Rev.*, *126*, 447–467.

Gonzalez-Galindo, F., F. Forget, M. A. Lopez-Valverde, M. Angelats i Coll, and E. Millour (2009), A ground-to-exosphere general circulation model: 1. Seasonal, diurnal, and solar cycle variation of thermospheric temperatures, *J. Geophys. Res.*, *114*, E04001, doi:10.1029/2008JE003246.

Gustin, J., B. Bonfond, D. Grodent, and J. C. Gerard (2012), Conversion from HST ACS and STIS auroral counts into brightness, precipitated power, and radiated power for H_2 giant planets, *J. Geophys. Res.*, *117*, A07316, doi:10.1029/2012JA017607.

Hodges, R. R. (1999), An exospheric perspective of isotopic fractionation of hydrogen on Venus, *J. Geophys. Res.*, *104*, 8463–8472, doi:10.1029/1999JE900006.

Hunten, D. M. (1973), The escape of light gases from planetary atmospheres, *J. Atmos. Sci.*, *30*, 1481–1494.

Hunten, D. M., and M. B. McElroy (1970), Production and escape of hydrogen on Mars, *J. Geophys. Res.*, *75*, 5589–6001.

Jakosky, B. M., and R. J. Philips (2001), Mars' volatile and climate history, *Nature*, *412*, 237–244.

Krasnopolsky, V. A. (2002), Mars' upper atmosphere and ionosphere at low, medium and high solar activities: Implications for evolution of water, *J. Geophys. Res.*, *107*(E12), 5128, doi:10.1029/2001JE001809.

Krasnopolsky, V. A. (2010), Solar activity variations of thermospheric temperatures on Mars and a problem of CO in the lower atmosphere, *Icarus*, *207*, 638–647.

LeBlanc, F., J.-Y. Chaufray, O. Witasse, J. Lilensten, and J.-L. Bertaux (2006), The Martian dayglow as seen by SPICAM UV spectrometer on Mars Express, *J. Geophys. Res.*, *111*, E09S11, doi:10.1029/2005JE002664.

LeBlanc, F., J.-Y. Chaufray, and J.-L. Bertaux (2007), On Martian nitrogen dayglow emission observed by SPICAM UV spectrograph/Mars Express, *Geophys. Res. Lett.*, *34*, L02206, doi:10.1029/2006GL028437.

Maltagliati, L., F. Montmessin, A. Fedorova, O. Korablev, F. Forget, and J.-L. Bertaux (2011), Evidence of water vapor in excess of saturation in the atmosphere of Mars, *Science*, *333*, 1868–1871.

Maltagliati, L., F. Montmessin, O. Korablev, A. Fedorova, F. Forget, A. Määttänen, F. Lefèvre, and J.-L. Bertaux (2013), Annual survey of water vapor vertical distribution and water aerosol coupling in the Martian atmosphere observed by SPICAM/MEX solar occultations, *Icarus*, *223*, 942–862.

McElroy, M. B. (1972), Mars: An evolving atmosphere, *Science*, *175*, 443–445.

McElroy, M. B., and T. M. Donahue (1972), Stability of the Martian atmosphere, *Science*, *177*, 986–988.

Montabone, L., E. Millour, F. Forget, and S. R. Lewis (2012), EPSC abstracts vol. 7, EPSC2012-773-1.

Owen, T. (1992), The composition and early history of the atmosphere of Mars, in *Mars*, edited by H. H. Kieffer et al., pp. 818–834, Univ. Arizona Press, Tucson.

Parkinson, T. D., and D. M. Hunten (1972), Spectroscopy and acronomy of O_2 on Mars, *J. Atmos. Sci.*, *29*, 1380–1390.

Rottman, G. J., N. W. Thomas, and W. McClintock (2006), SORCE solar UV irradiance results, *Adv. Space Sci.*, *37*, 201–208.

Thomas, G. E. (1963), Lyman alpha scattering in the Earth's hydrogen geocorona 1, *J. Geophys. Res.*, *68*, 2639–2660, doi:10.1029/JZ068i009p02639.

Villanueva, G. L., M. J. Mumma, R. E. Novak, H. U. Käufl, P. Hartogh, T. Encrenaz, A. Tokunaga, and A. Khayat (2015), Strong water isotopic anomalies in the Martian atmosphere: Probing current and ancient reservoirs, *Science*, *348*(6231), 218–221, doi:10.1126/science.aaa4326.

Yamauchi, M., T. Hara, R. Lundin, E. Dubinin, A. Fedorov, R. Frahm, Y. Futaana, M. Holmstrom, and S. Barabash (2015), Strong seasonal variations of Martian pick-up ions and reflected ions, Geophys. Res. Abstracts, vol. 17, EGU2015-4117.